A highly sensitive multi-element HgCdTe e-APD detector for IPDA lidar applications

Jeff Beck[1], Terry Welch[1], Pradip Mitra[1], Kirk Reiff[2], Xiaoli Sun[3], James Abshire[3]

[1] *DRS Technologies, Network and Imaging Systems, Inc., Dallas, TX,* [2] *Analog/Digital Integrated Circuits, Longwood, FL,* [3] *NASA Goddard Space Flight Center, Greenbelt, MD*
Contact Information: email *jeff.beck@drs.com, 972-560-2339 (office) 972-560-6104 (fax)*

Submitted for review to *Journal of Electronic Materials,* October 2013.

ABSTRACT

A HgCdTe e-APD detector has been developed for lidar receivers one application of which is integrated path differential absorption lidar measurements of atmospheric trace gases such as CO2 and CH4. The HgCdTe APD offers a wide, visible to MWIR, spectral response, high dynamic range, substantially improved sensitivity, and an expected improvement in operational lifetime. A demonstration sensor-chip assembly consisting of a 4.3 µm cutoff HgCdTe 4x4 APD detector array with 80 µm pitch pixels and a custom CMOS readout integrated circuit was developed. One typical array demonstrated APD gain of 654 at 12 V with corresponding gain normalized dark currents ranging from 1.2 fA to 3.2 fA. The 4x4 detector system was characterized at 77K with a 1.55 µm wavelength, 1 µs wide, laser pulse. The measured unity gain detector photon conversion efficiency was 91.1%. At 11 V bias the mean measured APD gain at 77 K was 307.8 with σ/mean uniformity of 1.23%. The average, noise bandwidth normalized, system NEP was 1.04 fW/Hz$^{1/2}$ with a σ/mean of 3.8%. The measured, electronics limited, bandwidth of 6.8 MHz was more than adequate for 1 µs pulse detection. The system demonstrated an NEP (3 MHz) of 0.4 fW/Hz$^{1/2}$ at 12 V APD bias and a linear dynamic range close to 1000. A gain independent quantum limited SNR of 80% of full theoretical indicated a gain independent excess noise factor very close to 1.0 and the expected APD mode quantum efficiency.

Keywords: HgCdTe, APD, NEP, IPDA, CO2, lidar

1. INTRODUCTION

NASA Goddard Space Flight Center (GSFC) is currently developing an integrated path differential absorption (IPDA) lidar that measure the column absorption of CO2 at 1572 nm, and CH4 at 1651 nm as candidates for NASA's Active Sensing of CO2 Emission over Days, Nights, and Seasons (ASCENDS) space mission. Both the CO2 and CH4 lidar measurements have been demonstrated from aircraft. One of the major technical challenges for the ASCENDS mission has been the lidar detector, that ideally has high photon sensitivity in this spectral region, a large linear dynamic range, along with a long in-space operational lifetime.

We have adapted the DRS HgCdTe e-APD detector for this application. The HgCdTe electron avalanche photodiode (e-APD) is a unique APD that provides high gain and high sensitivity from the visible to IR regions. This APD detector is attractive since its gain is nearly "noiseless" (the excess noise factor is close to unity) and is very uniform [1]. It can provide analog response with sensitivities in the photon counting level from the visible to the mid-IR. This offers improved sensitivities for lidar receivers as well as for other electro-optical systems applications.

The HgCdTe APD, detector design is based on the highly successful High Density Vertically Integrated Photodiode (HDVIP®) architecture. The HDVIP device is a front-side illuminated, cylindrical, p-around-n photodiode that is formed around a small via in the HgCdTe, shown in Figure 1 and Figure 2, where the via serves as the interconnect conduit between the n-side of the photodiode and the input to the readout circuit [2]. The HDVIP structure is currently employed in MWIR and LWIR staring arrays in production at DRS. The keys to the success of this architecture are: 1) interdiffused CdTe passivation of both surfaces for low 1/f noise, 2) thermal cycle reliability that is detector and array

size independent, 3) low defects due to diode junction orientation with respect to threading dislocations, 4) front side illumination for high quantum efficiency from 4 µm into the visible region, and good MTF [2].
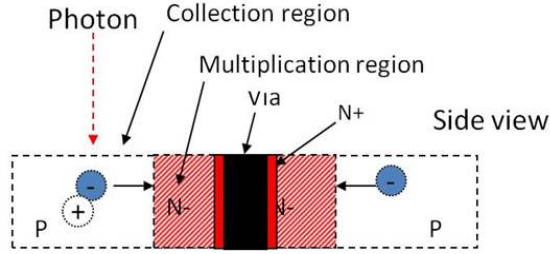

Figure 1   HDVIP APD cross section.   The p region is the absorption region and the n- region is the multiplication region.
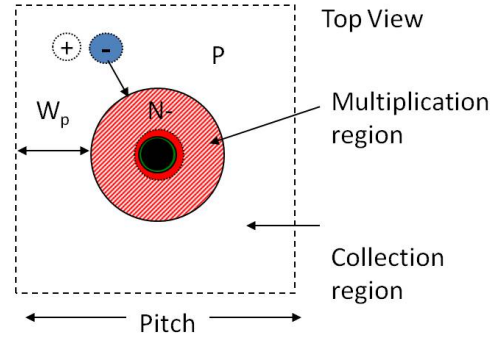
Figure 2   Top view of HDVIP APD unit cell

For APD operation the reverse bias is increased until an electric field sufficient for avalanche multiplication is achieved. At a few volts bias, the n- region becomes fully depleted [2].   Photo-electrons generated in the p region diffuse to the n region, which is the multiplication region. A unique feature of the HgCdTe e-APD is that holes generated in the multiplication region, for all practical purposes, do not multiply which results in an ideal k = 0 APD where k is the hole to electron ionization coefficient ratio. Another unique feature of the HgCdTe e-APD is that the multiplication process is largely deterministic [3,4] which results in an excess noise factor near 1.0.

The HgCdTe e-APD has shown high, uniform, exponential gain without breakdown.   Also, the HgCdTe e-APD exhibits a gain independent excess noise factor [1]. These characteristics, exponential gain without breakdown, and a gain independent excess noise factor are predicted for an "ideal" k=0 APD. The near 1.0 excess noise factor is the result if a deterministic (history dependent) ionization process.

This performance has been realized in large and small area array formats. Range gated imaging, 128x128 40 µm pitch, focal plane arrays (FPAs) demonstrated sub 0.5 photon noise equivalent input sensitivities with a median APD gains as high as 946 [5]. Linear mode single photon detection with high single photon signal to noise ratio, average value of 13.7, less than 1ns jitter, and a photon detection efficiency near 50% has been demonstrated in a 2x8 array operating at an APD gain near 500 [6].

Initial results on the 4x4 APD SCA, the subject of this paper, were presented at the 2013 SPIE DSS meeting in April-May of 2013 [7]. In this paper we summarize those findings, and provide additional results obtained since then.

2.   DESIGN OF LIDAR DETECTOR

2.1 Requirements

This application is for an IPDA lidar that transmits 1 µs wide laser pulses with ~50 ns rise times. Therefore, the design goal was to achieve an optimized noise equivalent power (NEP) for a bandwidth of 3-8 MHz. Based on simulations of ROIC performance (discussed in Section 2.3), an assumed worst worse case detector net photon conversion efficiency of 50%, three gain normalized dark currents, and Dewar optics transmission, we calculated the expected system NEP as a function of APD gain shown in Figure 3 for the baseline ROIC gain setting. This modeling showed that with this conservative set of assumptions an NEP of < 5 fW/Hz$^{1/2}$ could be achieved with APD gains of around 100 with an effective gain normalized dark current (GNDC) of less than 64 pA, a 9.8 MHz bandwidth, and transimpedance preamp with a gain of 330 kV/A and broadband RMS noise of 340 µV. NEP performance approaching 1 fW/Hz$^{1/2}$ was expected for higher APD gains and lower dark currents.

2

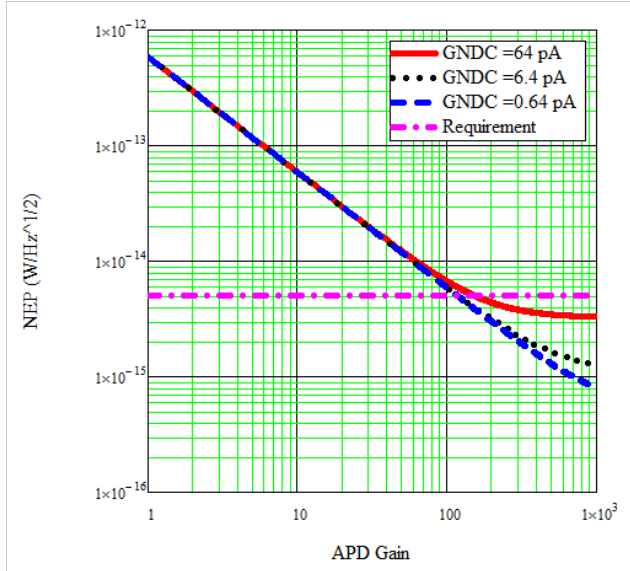Figure 3 Predicted NEP for 9.8 MHz bandwidth

2.2 Array and Fanout

The array consisted of a 4x4 arrangement of square 80x80 μm pixels on an 80 μm pitch. The array was fabricated on a SiO$_2$/Si fanout that provided connections from the array to bond pads for interconnect to the ROIC. The array is surrounded by a ring of guard diodes surrounded by a substrate contact ring. Each pixels consists of 4 APDs on a 40 μm pitch, in a 2x2 arrangement, connected in parallel be means of underlying metallization on the fanout.   The fanout was designed to provide a minimum stray input capacitance from the detector, to the bond pads.   To do this, minimal trace lengths and trace widths, and small bond pads, were used.

2.3 Preamplifier (ROIC)

The ROIC is a custom CMOS design that uses 0.18 μm design rules. The unit cell consists of a resistive transimpedance amplifier (RTIA) connected to the cathode of the APD that provides signal input. Three selectable feedback resistors set the option of 7 transimpedance gain values. There is also the option of running in a capacitive transimpedance amplifier (CTIA) mode.   The preamp is followed by a sample and hold circuit and a post-amp buffer stage with three selectable gain settings of 1, 2 and 4 V/V. The sample and hold is used in the CTIA mode.   The combination of the preamp and post amp gain selections results in 21 possible full path transimpedance gains in the design that range from 47.7 kΩ to 1325 kΩ, a factor of 27.8. The design baseline was a full path gain of 331 kΩ with a 1x buffer gain setting.   End to end performance simulations were carried out which assumed a worst case input capacitance. These simulations predicted that the bandwidth would range from 21.9 MHz at the lowest gain to 8.9 MHz at the highest gain. The baseline design gain was 331 kΩ at 80K; the predicted full path integrated noise was 336 μV; the 3dB signal bandwidth was 9.77 MHz; and the shot noise was 115.2 fA/Hz$^{1/2}$ at 100 KHz. The noise bandwidth was predicted to be 1.17 times the signal bandwidth.

The ROIC passed room temperature design verification testing at 25 C in RTIA mode with measured performance very close to simulation predictions.   The pulse rise time, with the 320 KΩ 1x post amp gain setting, implies a bandwidth of 9.2 MHz which is close to the predicted cold value of 9.8 MHz. Dynamic range measurements showed a 2V peak to peak swing. With an adjustable APD gain from 1 to 300 and the minimum to maximum ROIC gain, the dynamic range is expected to be greater than 70 dB from the noise level.

At DRS the ROIC was tested with a detector array. Proper operation, gain setting functionality, noise, and bandwidth were verified. With an 8x gain buffer board, the measured broadband noise with the baseline preamp gain settings was 302 μV which is lower, than the predicted simulation value of 336 μV. The rise time with this gain setting was 51 ns for a bandwidth of 6.8 MHz.

2.4 Dewar and Optics

A closed cycle, reconfigurable, Dewar with a 1.5 watt cryocooler was selected for operation at temperatures near 80K. The cold shield was designed to accommodate a F/1.5 optical cone and a 25.4 mm diameter cold filter. A 1.2 to 1.8 μm bandpass filter with OD4 blocking from 3 to 5 μm was selected for testing with 1.55 μm laser signals at DRS. The Dewar had two multi-pin connectors for I/O.

2.5 Electronics and Software

A custom set of 4 electronic printed circuit boards were designed and fabricated: 1) an internal Dewar board; 2) an external Dewar interface card with buffers for the analog signals; 3) a second external Dewar interface card for digital control and power; 4) a power, command, and control, side-board. The internal Dewar board holds the 68 pin LCC and provides the electrical interface between the LCC and the two Dewar connectors. The two external Dewar interface

cards attach directly to the two Dewar connectors.   The side-board is connected to the interface cards with ribbon cables. FPGA code and software were written to provide a control from using a laptop PC connected by a USB port to the side-board. Two analog buffer cards were fabricated: one with a 1x gain into 50 Ω and another with an 8x gain.

3.   4X4 ARRAY FABRICATION AND TEST

A fabrication lot was run with 96 4x4 arrays on 16 HgCdTe chips. The arrays were screened by measuring dark current voltage data out to 10 V on the center four pixels of each array at 77 K.   Sixty-six arrays (69%) met the dark current requirement in the center four pixels. Eleven of these were selected for full 16 pixel characterization. Five "perfect" arrays were found in which all pixels met 6.4pA maximum GNDC spec at 10 V where the APD gain was assumed to be around 160.[1] The data are summarized in Table 1. Four of these five arrays had pixels with gain normalized dark currents no higher than 67 fA. The center 4 pixels in these 4 arrays had gain normalized dark currents less than 8.6 fA, that is almost 0.1% of the baseline design requirement.

Gain and dark current were measured as a function of bias on several arrays. Array A8052-2C had a gain of 173 at 10 V. The GNDC at 10 V was about 4 fA, which is well below the flow down baseline requirement of 6400 fA. A8052-2A had a gain at 10 V of 157 and a GNDC of 18 fA. Another fanout array, A8052-15D, was measured for gain and dark current out to 12 V. The data shown in Figure 4 and Figure 5 reveal a gain of 144 at 10 V, a gain of 654 at 12 V, and a GNDC of 1.2 to 3.2 fA at 12 V. In conclusion, based on dark current and gain measurements, the 4x4 fanout lot produced excellent dark current results with very good yield. Based on the model shown in Figure **3**, noise bandwidth normalized system NEPs of 1 fW/Hz$^{0.5}$ were predicted to be with reach.

Table 1 Gain normalized dark current at 10 V of 5 "perfect" fanout arrays (gain of 160 assumed)

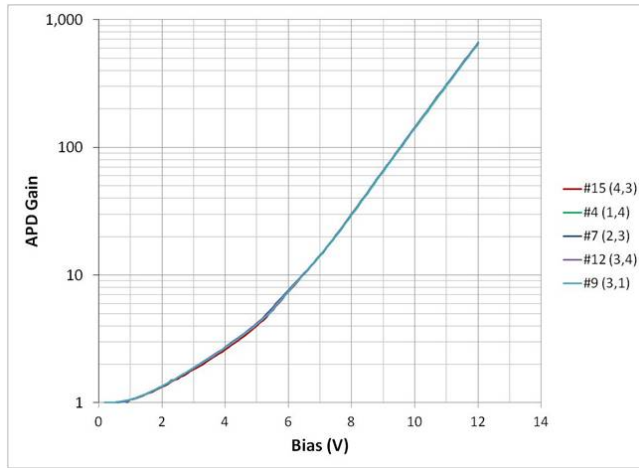| Array	Median GNDC (fA)	Max GNDC (fA)	Max GNDC (center 4) (fA)
4E	1.64	3.94	1.3
11D	1.43	20.4	8.53
7C	0.883	8.11	1.7
13E	3.49	66.8	8.13
16B	5.46	7540	8.06

Figure 4 Gain vs. voltage on four pixels from detector array A8052-15D to 12 V. Gain of 654 at 12 V.
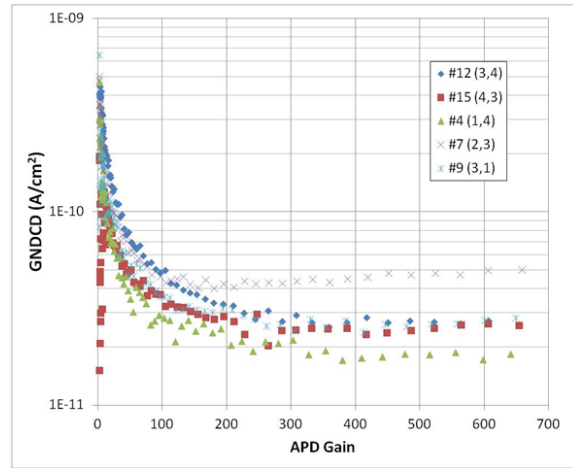

Figure 5   Gain normalized dark current density vs. gain on pixels from detector array A8052-15D. (Below a gain of ~ 200 the dark currents were below the system measurement limit.)

---

[1] The gain of 160 used in the calculation of gain normalized dark current is based on measured gains from 157 to 173 on two arrays 2A and 2C from this lot.   It should be fairly close to the gain for all arrays in the lot since the cutoffs are the nearly the same (4.27 to 4.35 μm).

4

4. SCA TEST RESULTS

4.1 Sensor Chip Assembly

The five selected fanout arrays were integrated with tested ROIC chips in a 68 pin LCC. The layout is shown in Figure 6. Array A8052-4E was selected for test and delivery with the system.

4.2 System Integration

The 4x4 array detector system, consisting of the Dewar, cooler, optics, electronics boards, and SCA, was assembled. The system test configuration at NASA GSFC is shown in Figure 7.
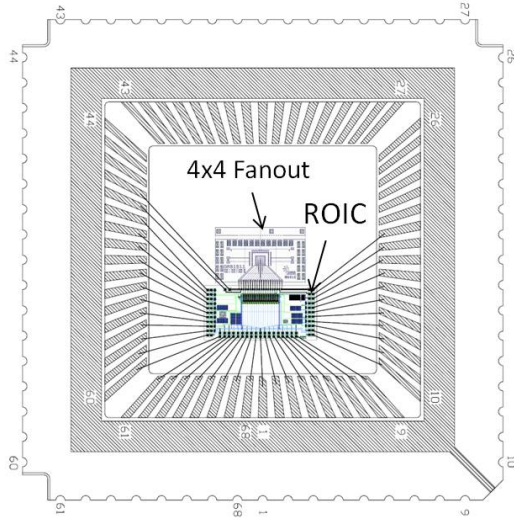

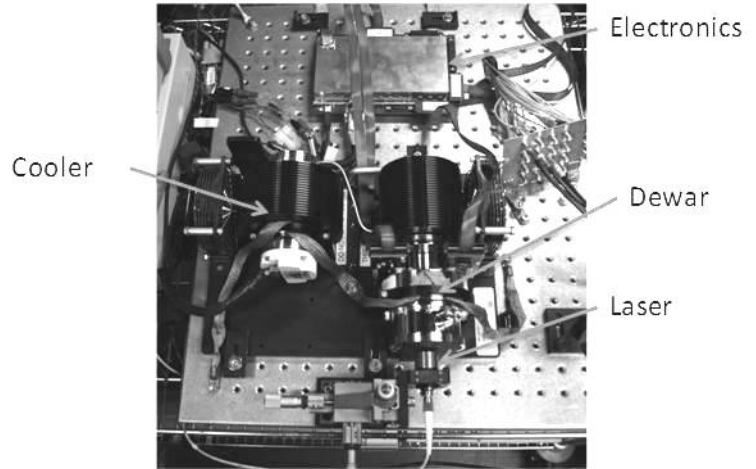Figure 6 Sensor chip assembly layout. The 4x4 array is centered in the LCC

Figure 7 The 4x4 APD array detector system test configuration at GSFC

4.3 Test Results

We first performed some basic characterization measurements. The system test conditions are summarized in Table 2. Shown in Figure 8 is the measured APD gain vs. bias on one of the pixels, pixel 9 (row 3, column 1) at 77K. The gain at 10 V was 141 and at 11 V it was 297. The photon-to-electron conversion efficiency, CE, at unity gain was calculated from the measured signal data at a bias of 0.5 V where the APD gain is 1. The calculation assumes the expected end-to-end gain of 330kV/Amp based on the measured room temperature values with a predicted 3% increase at 77K. The data show an average CE of 91.1% and a 1.5% σ/mean uniformity. Correcting for the unity gain fill factor of 0.98, the active region QE is 93%.

The rise times were measured on all 16 pixels at 77 K with a 10 V bias applied. The rise times varied from 49.6 ns to 51.8 ns with an average of 50.9 ns for a bandwidth of 6.79MHz. The noise bandwidth used in the NEP/Hz$^{1/2}$ calculations was estimated from ROIC simulations to be 8.14 MHz. Shown in Figure 10 is the measured gain at 10 V and 11 V on all pixels at 77 K. At 10 V the APD gain was 146.0 with a σ/mean of 1.31% At 11 V the average gain increased to 307.8 with a σ/mean of 1.23%.

We measured the system NEP at APD biases of 10V and 11 V at 77 K with an external buffer gain of 8 V/V. The average responsivity at 11 V was 782.0 µV/pW with a 1.8% σ/mean. The corresponding detector responsivity at 11 V was 355 A/W. The average broadband NEP at 11 V was 2.97 pW. The estimated NEP/Hz$^{1/2}$ is calculated by dividing the NEP by the noise bandwidth which is estimated to be 1.2 times the signal bandwidth. The NEP for each pixel, shown, in Figure 9, indicates an average NEP at 11 V of 1.04 fW/Hz$^{1/2}$ with a 3.8% σ/mean and 100% pixel operability with no pixel having an NEP less than 1.12 fW/Hz$^{1/2}$.

5

At 10 V the APD gain decreased to 145 and the NEP increased to 2.20 fW/Hz$^{1/2}$. This indicates that the NEP is changing directly with APD gain. Therefore, further reduction in the NEP is expected with increased bias beyond 11 V.

Table 2 Test conditions for NEP data

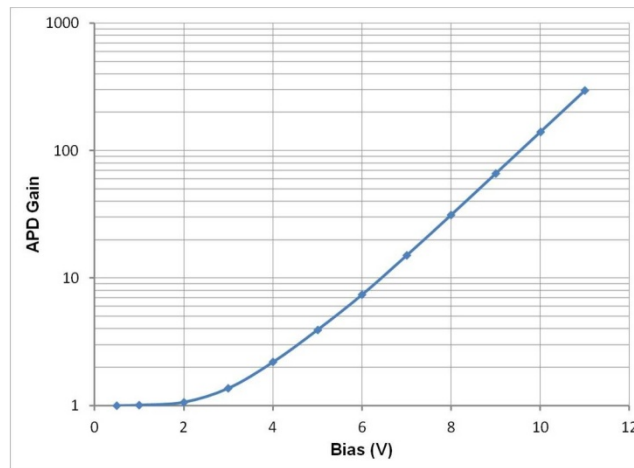| Parameter	Value	Units
Signal wavelength	1.55	μm
Signal pulse width	1	μs
Signal amplitude	< 2-100	nW
Operating temperature	77	K
ROIC Preamp gain	330	kW
ROIC postamp gain	1	V/V
Dewar buffer card gain into 1MΩ	8	V/V
Cold Filter pass band	1.2-1.8	μm
Cold filter transmission @ 1.55 μm	86	%
Cold filter blocking 3-5 μm	OD4	NA
Dewar window transmission	97	%

Figure 8 Gain vs. Bias for A8052-4E pixel 9 at 77 K.
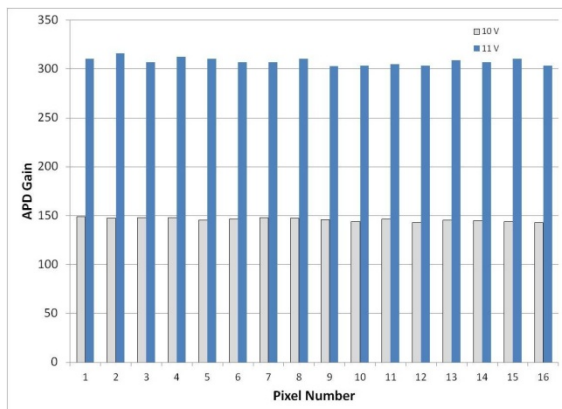

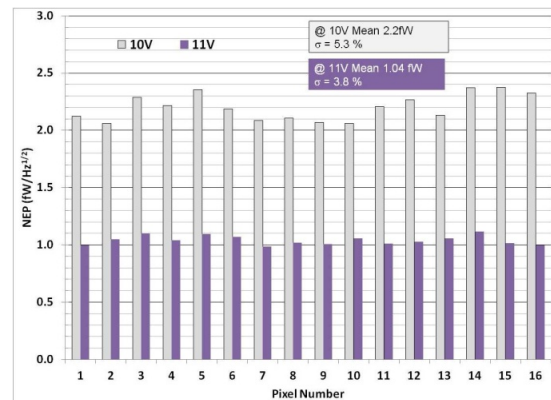Figure 10 APD gain at 10V and 11 V vs. pixel at 77K for array A8052-4E

Figure 9 System NEP vs. pixel at 10 V and 11 V bias at 77 K (A8052-4E)

4.4 Test Results at NASA GSFC

Measurements at GSFC verified and added to the results obtained at DRS. The measured NEP/Hz$^{1/2}$ and responsivity vs. APD bias, plotted in Figure 11, shows an NEP at 3 MHz of 0.7fW/Hz$^{1/2}$ at 11V and 0.4 fW/Hz$^{1/2}$ at 12 V.

A near-linear dynamic range over three orders of magnitude was measured, as shown in Figure 12. In this case the dynamic range was measured at the highest ROIC transfer gain of 331 KV/A (77 K gain) and an post-amp gain of 1 and the APD gain of 308 corresponding to 11 V bias. The 1.3 V upper limit of the dynamic range was limited by the swing of the external buffer amplifier.
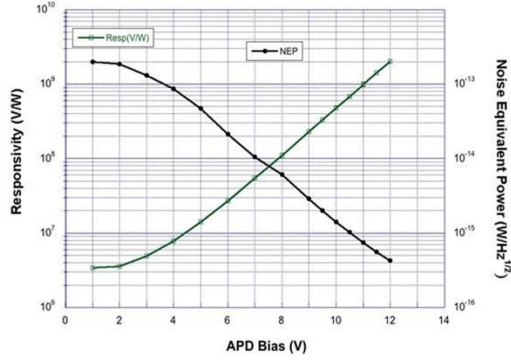

Figure 11 **Measured Responsivity and NEP (W/Hz$^{1/2}$) at 1.55 μm** at 3 MHz vs. bias

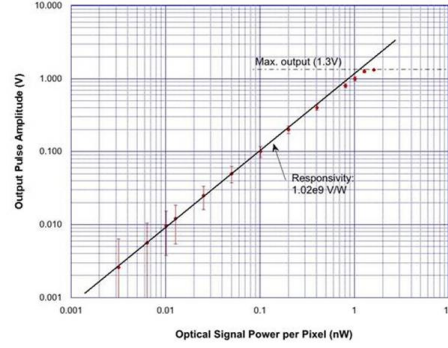Figure 12 **Dynamic Range Measurement**: Output Pulse amplitude vs. incident power/pixel @ 11V.0 APD bias, 1 μs rectangular pulse and RTIA gain set to 320 kV/A

Measurements at GSFC of the detector's signal to noise ratio (SNR) vs. APD bias for three signal levels are shown in Figure 13 where both the signal and noise are measured under flux. It was seen that the *SNR* reached a constant, gain independent, limiting value that was about 81% of the quantum limit, *QL*, where the normalized quantum limit for an APD with excess noise *F(M)* is given by:

$$QL = \sqrt{\frac{QE \times FF_{APD}}{F(M)}} = \sqrt{\frac{CE_{APD}}{F(M)}}$$

where *QE* is the net photon to electron conversion efficiency in the absorption region (p-region), and *FF$_{APD}$* is the APD fill factor which excludes the area of the multiplication region (n-region) and via (see Figure 2). The pixel incident photon to electron conversion efficiency at high gain, *CE$_{APD}$*, is the product of the *QE* and the APD fill factor. The bias independence in the high bias region of Figure 13 is due to the gain independence of the excess noise factor. With a quantum limited SNR of 16 (0.813 of full theoretical), an APD fill factor of 0.74 and a *QE* of 0.93, the calculated excess noise factor comes out close to 1.04.[2]
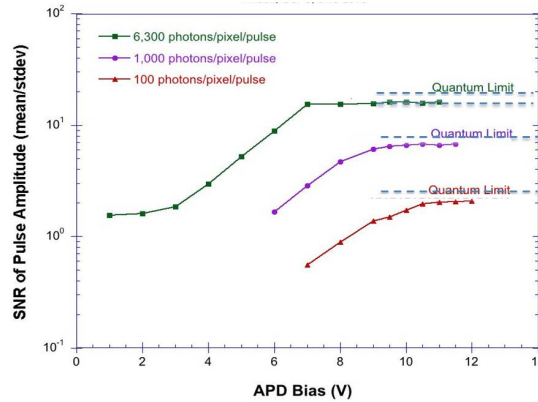

Figure 13 **Measured SNR vs. bias showing quantum limit** with 1 μs rectangular pulse

---

[2]   The APD fill factor is the fill factor predicted from the 23 μm n-region diameter and the 40x40 μm APD pitch.

4.5 Post Delivery Test Results at DRS

The four remaining SCA's were measured at DRS in a second system. The system is identical to the first except the buffer gain was 10.7 instead of 8. All four SCAs exceeded the 5 fW/Hz$^{1/2}$ requirement by a large margin with 100% pixel NEP operability (no pixels in any array having a max NEP greater than 20% of the mean NEP for that array). The range of demonstrated NEPs varied from 1.60 to 0.62 fW/Hz$^{1/2}$. Two of these SCA were tested at 12 V APD bias and both achieved measured mean broadband noise normalized NEPs less than 1 fW/Hz$^{1/2}$. The one SCA had a mean broadband noise-bandwidth normalized NEP of 0.66 fW at 12V which appeared to be limited by a very low background flux in the Dewar. In fact, single photon sensitivity was seen in this array at 12 V with an average single photon SNR roughly around 3.5, which is in the ball park of the predicted SNR.

5. SUMMARY

We have developed and characterized a new, highly sensitive, 4x4 HgCdTe e-APD array optimized for 1 μs lidar pulse detection and packaged with Dewar, cooler, and electronics. The APD fabrication process demonstrated a high array yield, very low dark currents, and 100% pixel NEP operability on the 5 assembled SCAs whereby all the pixel NEPs were tightly distributed about the mean NEP.

The measured performance at 77 K of the delivered SCA is summarized Table 4 for the set of conditions listed in Table 3. The delivered SCA has an average NEP of 1.04 fW/Hz$^{1/2}$ at 11V bias, very good gain, responsivity, and NEP uniformity (100% of the pixels with NEP $\leq$ 1.12 fW/Hz$^{1/2}$). The measured bandwidth was 6.8 MHz (design goal 4 MHz) and the NEP was a factor of 5 better than the design requirement. The dynamic range for the minimum to maximum ROIC gain and a variable APD gain from 1 to 300 is 70 dB, measured from the noise level. The measurement results showed good agreement with performance predictions.

Table 3 Operating conditions for detector NEP characterization (Table 4)

Parameter	Value	Comment
FPA Temperature	77 K	Initial setting during cooler check-out
ROIC Gain	331 kΩ	Predicted for 80 K (320 KΩ @ 300K)
ROIC post amp gain	1	
Buffer Gain	8	50 Ohm load
Laser pulse width	1 μs	

Table 4 System performance at 1.55 μm with Baseline RTIA Gain Setting

Parameter	Value	Comment
APD Bias	11 V	Applied to all pixels
APD Gain	308	Average
NEP at 1.55 μm	2.97 pW	Broadband NEP
NEP/Hz$^{1/2}$	1.04 fW/Hz$^{1/2}$	Normalized to noise bandwidth
Responsivity at 1.55 μm	782 μV/pW	At system output
Noise at 11 V	2.32 mV	At system output (gain of 8)
System Noise (@ 0.5 V)	2.41 mV	At system output (gain of 8)
Bandwidth	6.8 MHz	51 ns rise time
Noise bandwidth	8.1 MHz	Based on predicted 1.2 factor
Dynamic Range (dB)	72	APD gain 1-300; min to max ROIC gain

8

6. FUTURE PLANS

GSFC plans to integrate the delivered detector, Dewar, cooler, and electronics assembly into their airborne IPDA lidar and to demonstrate measurements of CO2 over horizontal paths and from an aircraft. GSFC also plans to examine and characterize the single photo sensitivity.

7. ACKNOWLEDGEMENTS

The authors would like to acknowledge the important contributions of DRS employees James McCurdy (testing), Chris Kamilar (electronics), Mark Skokan (fanout array design), Richard Scritchfield (consulting), Drew Gordon (software), Patty Benken (array fabrication), and Towfik Teherani (management support).

[1] J. Beck, C. Wan, M. Kinch, J. Robinson, P. Mitra, R. Scritchfield, F. Ma, J. Campbell, "The HgCdTe Electron Avalanche Photodiode", J. Elecron. Mater. 35, No. 6, 1166 (2006)

[2] J. Beck, et. al, "Performance and Modeling of the MWIR HgCdTe e-APD", J. Elecron. Mater. 38, No. 8, 1579-1592 (2009)

[3] M. Kinch, "A Theoretical Model for the HgCdTe Avalanche Photodiode", J. Elecron. Mater. 37, No. 9, 1453 (2008)

[4] J. Rothman, L. Mollard, S. Goût, J. Wlassow, "History dependent impact ionization theory applied to HgCdTe e-APDs", J. Elecron. Mater. 40, No. 8, 1757-1768 (2011)

[5] J. Beck, M. Woodall, R. Scritchfield, M. Ohlson, L. Wood, P. Mitra, and J. Robinson, "Gated IR Imaging with 128x128 HgCdTe Electron Avalanche Photodiode FPA", Proc. SPIE, 654217, 1-17 (2007).

[6] J. D. Beck, R. Scritchfield, P. Mitra, W. Sullivan III, A. D. Gleckler, R. Strittmatter Robert J. Martin, "Linear Mode Photon Counting with the Noiseless Gain HgCdTe e-APD", Proc. SPIE, 80330N, 1-15 (2011)

[7] J. Beck, J. McCurdy, M. Skokan, C. Kamilar, R. Scritchfield, T. Welch, P. Mitra, X. Sun, J. Abshire*, K. Reiff, "A highly sensitive multi-element HgCdTe e-APD detector for IPDA lidar applications", Proc. SPIE Vol. 8739, 87390V (2013)